Construction and Building Materials 402 (2023) 132958

Contents lists available at ScienceDirect

Construction and Building Materials

journal homepage: www.elsevier.com/locate/conbuildmat

Clinker Portland with iron ore tailing and its characterization by integrated laboratory methods

Natacha C. N. Faria [a], Valdir M. Pereira [a], Thiago R. S. Nobre [a], Roberto Cesar de O. Romano [a], Antonio C. Vieira Coelho [b], Sergio C. Angulo [a,*]

[a] Department of Construction Engineering, Polytechnic School, University of São Paulo (USP), São Paulo, Brazil
[b] Department of Materials and Metallurgical Engineering, Polytechnic School, University of São Paulo (USP), São Paulo, Brazil

ARTICLE INFO

Keywords:
Iron ore tailings
Clinker Portland
Reduced-scale laboratory tests

ABSTRACT

The large volume accumulation of iron ore tailings (IOT) in Brazil poses significant risks of accidents, highlighting the need for strategies for their recycling. The Brazilian's IOT possesses mainly iron oxide content (HI-IOT) and can be used as raw materials alternatives in clinker production. Based on a fixed lime saturation factor (LSF = 0.96), we incorporated 5 to 10 wt% of HI-IOT in the raw meal to produce Portland clinkers. The mineralogical phases (alite, belite, aluminate, and ferrite) were evaluated by quantitative X-ray diffraction. Optimal results were obtained with 7.5 wt% of HI-IOT in the clinker Portland, i.e., approximately 32 %wt. of clay substitution. The mechanical strength evolution was evaluated by a reduced-size test and obtained compressive strength of 34.8 MPa at 3 days-age, 54.10 MPa at 7 days-age, and 71.20 MPa at 28-days values compatible with standardized high initial strength Portland cement. By monitoring the complete hydration process using TG/DTG and assessing the volumetric composition over time, valuable insights were gained regarding the potential application of these Portland cements at an industrial scale.

1. Introduction

Mining activities in Brazil generate a large volume of iron ore tailings (IOT) which poses a danger if not properly managed. The accumulation of tailings in dams (a non-circular strategy) can lead to disasters, such as the loss of human lives, immense environmental damage, and economic and financial consequences [1–3]. These events highlight the importance of finding ways to recycle and manage the IOT in Brazil and other places where these natural resources are explored. This approach is necessary to reduce the risks of future disasters, and it is a substantial step toward sustainability and preserving the environment, as also to apply a circular economy approach [4,5].

Use of mining tailings such as an alternative raw material for clinker production conserves non-renewable natural resources [6] like limestone and clays. So, it depends on the availability of its primary oxides (CaO, SiO_2, Al_2O_3, and Fe_2O_3) for clinker mineral phases formation. Various sources, such as *fly ash* (*bottom ash*) [7,8], waste from cementitious materials [9], tailings from different sources [10,11] and, even hazardous waste [12] have been successfully tested to produce clinker and used by industry.

The IOT can be a promising clinker raw material, but the location of the ore (the original rock) and processing processes will interfere with its chemical composition (Table S.1 - **Supplementary Data**). Countries such as China, Malaysia, and Australia have IOT with Fe_2O_3 contents that rarely exceed 25%, whereas a fine fraction of tailings with high iron oxide, above 40 wt%, are found in countries like Brazil and India [13]. Therefore, Brazilian IOT is composed predominantly by Fe_2O_3. In addition, SiO_2 and Al_2O_3 also are present [14–16]. This material, namely HI-IOT (iron ore tailing with high iron oxide), herein may limit the substitution of aluminosilicate-based raw material as clay by the HI-IOT. Studies about HI-IOT as raw material in clinker Portland are scarce in international literature (Table S.1 - **Supplementary Data**).

Particularly in Brazil, the use of HI-IOT in clinker production is not yet available. In this sense, there is doubt about the optimal replacement of usual raw materials or correctives (to adjust raw meal and clinker composition), and fully understanding its clinker Portland cement reactivity and evolution of mechanical strength. Studies in China have evaluated IOT use as an alternative raw material for clinker in the production of Portland cement and have shown optimal replacements of up to 10% [17,18], but China's IOT does not have high iron contents like

* Corresponding author.
E-mail address: sergio.angulo@usp.br (S.C. Angulo).

https://doi.org/10.1016/j.conbuildmat.2023.132958
Received 7 June 2023; Received in revised form 2 August 2023; Accepted 11 August 2023
Available online 22 August 2023

those from Brazil and did not test the reactivity of the clinker cement. Typically, most studies with HI-IOT have been appointed toward high-belite cement development [10,19], an unconventional Portland cement.

To incorporate IOT in Portland clinker adjusting the raw materials ratio in the "raw meal" is necessary to obtain a suitable quality. It involves monitoring and adjusting multiple interdependent variables such as chemical moduli (lime saturation factor (LSF), silica modulus (SM), alumina modulus (AM), and hydraulicity modulus (HM) and mineral phases levels, as alite, belite, aluminate, and ferrite [20]. Usually, the percentage of clinker mineral phases is estimated by Bogues's equations [21].

In our understanding, the main challenge in using HI-IOT as a raw material is to keep clinker reactiveness, adopting an LSF equal to or higher than 0.96 (recommended for clinker Portland) [22] for the "raw meal" as adopted in this manuscript. The HI-IOT use may guarantee a proper formation of liquid phases during the clinker formation. In addition, it can avoid additional correctives and clay use. In this scenario, the expected values of SM and AM need to be secured [23]. Finally, we tried to keep ferrite content under 12 – 15% [24] since changes in the mineralogy of the clinkers may affect the hydration evolution of the cement [25,26], which can retard its setting time and mechanical properties over time. The dosage protocol may increase the contents of IOTs in Portland clinkers development.

Most of studies from literature were done on a laboratory scale, with a few grams of samples, unable to measure the reactivity by calorimetry, or thermogravimetry (TG/DTG) hydration monitoring, or measure the strength of Portland clinker cement paste due to the mass required to produce mortar-scale specimens. Standard tests to evaluate strength require a high quantity of material (ten kilos or more) to do the tests. This restriction limits the scope of the results and, therefore, the applicability to the industry.

We evaluated herein the clinker reactiveness and the strength evolution using a small-scale laboratory test method. As far as we know, no other studies in the literature have integrated heat and TG/DTG monitoring to describe hydration kinetics and small-scale mechanical tests in cement pastes to comprehensively evaluate the technical feasibility of using HI-IOT for developing clinker Portland that meets commercial standards.

2. Experimental program, materials, and methods

2.1. Raw materials characterization

Raw materials used to prepare Portland cement clinker were natural clay, HI-IOT, and reagent-grade calcium carbonate (>98 wt% $CaCO_3$). The clay was provided by a ceramic industry, from Minas Gerais, state Brazil. The HI-IOT is a representative fine fraction (less than 0.1 mm) from a flotation process of a large iron ore mining operation. The HI-IOT used is part of a large-scale research study with the University of Sao Paulo to make a feasible solution for HI-IOT use in cementitious materials.

Tests of leaching were carried out in the HI-IOT (Table S.2 - **Supplementary Data**). The leaching of concerning elements did not exceed the limits and the HI-IOT could be characterized as a non-hazardous waste [27].

The chemical analysis of the raw materials was presented in Table 1**.** The oxides were determined by X-ray fluorescence (XRF) using a Malvern Panalytical equipment (Zetium model), with lithium tetraborate melted pastilles. The loss on ignition (LOI) was determined after calcination at 1,020 °C for 2 h. The HI-IOT and clay have iron oxide (Fe_2O_3), silica (SiO_2), and alumina (Al_2O_3). The clay and HI-IOT exhibited different silica and alumina modulus (SM and AM), with SM of 2.79 and 0.66, and AM of 3.85 and 0.28, respectively. The iron oxide content in HI-IOT was found to be approximately nine times greater than present in the clay; therefore, those needs limiting for full use as a carrier of these main oxides for clinker production.

The raw materials were mineralogically characterized by X-ray diffraction (XRD) powder analysis. The analysis was performed on a Panalytical X'Pert diffractometer, at room temperature, with CuKα radiation (λ = 1.5406 Å), except for HI-IOT that used the CoKα radiation (λ = 1.785 Å), both operating with a current of 40 mA, but with 45 kV for HI-IOT and 40 kV of voltage for the other raw materials (0.02 °2θ; 300-sec steps). The mineralogical analysis was performed using Panalytical's X'Pert HighScore Plus software (version 4.9) with Crystallography Open Database (COD) and Inorganic Crystal Structure Database (ICSD) files.

The Rietveld refinement [28,29] was realized to quantify the mineralogical phases of the raw materials (quantitative X-ray diffraction – QXRD). For all diffraction patterns, the general parameters refined were scale factor, background parameter with "use available background" function, zero shift error, unit cell, and peak shape parameters (W, V, and U) using the pseudo-Voigt function. The refinement ended with the application of preferred orientation, using the Spherical Harmonics function, only on compounds that tend to be oriented.

Fig. 1 presents the mineralogical phases and QXRD (Table S.3 - **Supplementary Data**), which reveals that both clay and HI-IOT contain common mineral species, such as kaolinite, quartz, dickite, and goethite. However, their contents were found to differ significantly. Iron oxide carrier minerals were found to be predominant in HI-IOT (goethite and hematite, essentially), which accounts for the high Fe_2O_3 content observed in the material.

The particle size distributions (PSD) of clay, HI-IOT, and $CaCO_3$ were obtained in a Helos HR, Sympatec laser granulometry (0.1 to 350 μm). Fig. 2 shows the volume and cumulative distribution of the particle sizes that lead to determining three characteristic diameters d_{10}, d_{50} and d_{90} for percentiles of 10%, 50%, and 90%, respectively. The particle size distribution of both clay and HI-IOT was found to be similar (Fig. 2**a**). This scenario leads to an appropriate sintering rate even for high-strength cement, as this property is generally inversely proportional to the particle size [20,30].

2.2. "Raw meal" mix proportion

Eight parameters were defined in dosage methodology, four related to the chemical moduli (Lime Saturation Factor - LSF, Alumina modulus - AM, Silica Modulus - SM, and Hydraulic Modulus - HM) and four related to the expected contents of the clinker minerals phases (C_3S, C_2S, C_3A, and C_4AF) (Table S.4 - **Supplementary Data**). The clinker acronym was CI_x, clinker with HI-IOT substitution (CI) and × represents the content of HI-IOT in raw meal resulting from clay replacement (Table 3).

The control variables herein were LSF and HM. The LSF value was kept above 0.96 (Table 2), which is within the normal range for clinker (0.92 to 0.98) [22], and the HM is kept within the recommended range

Table 1
Chemical analysis of raw materials by XRF (wt.%).

Raw materials	LOI	SiO_2	Al_2O_3	Fe_2O_3	CaO	MgO	Na_2O	K_2O	Others*
$CaCO_3$**	43.9	–	–	–	56.1	–	–	–	–
Clay	8.88	64.7	18.4	4.78	0.25	0.4	0.10	0.93	1.56
HI-IOT	8.94	35.1	11.5	41.8	0.10	0.13	0.10	0.10	2.28

* Others = contents below 0.01; ** Chemical composition by Rietveld refinement.

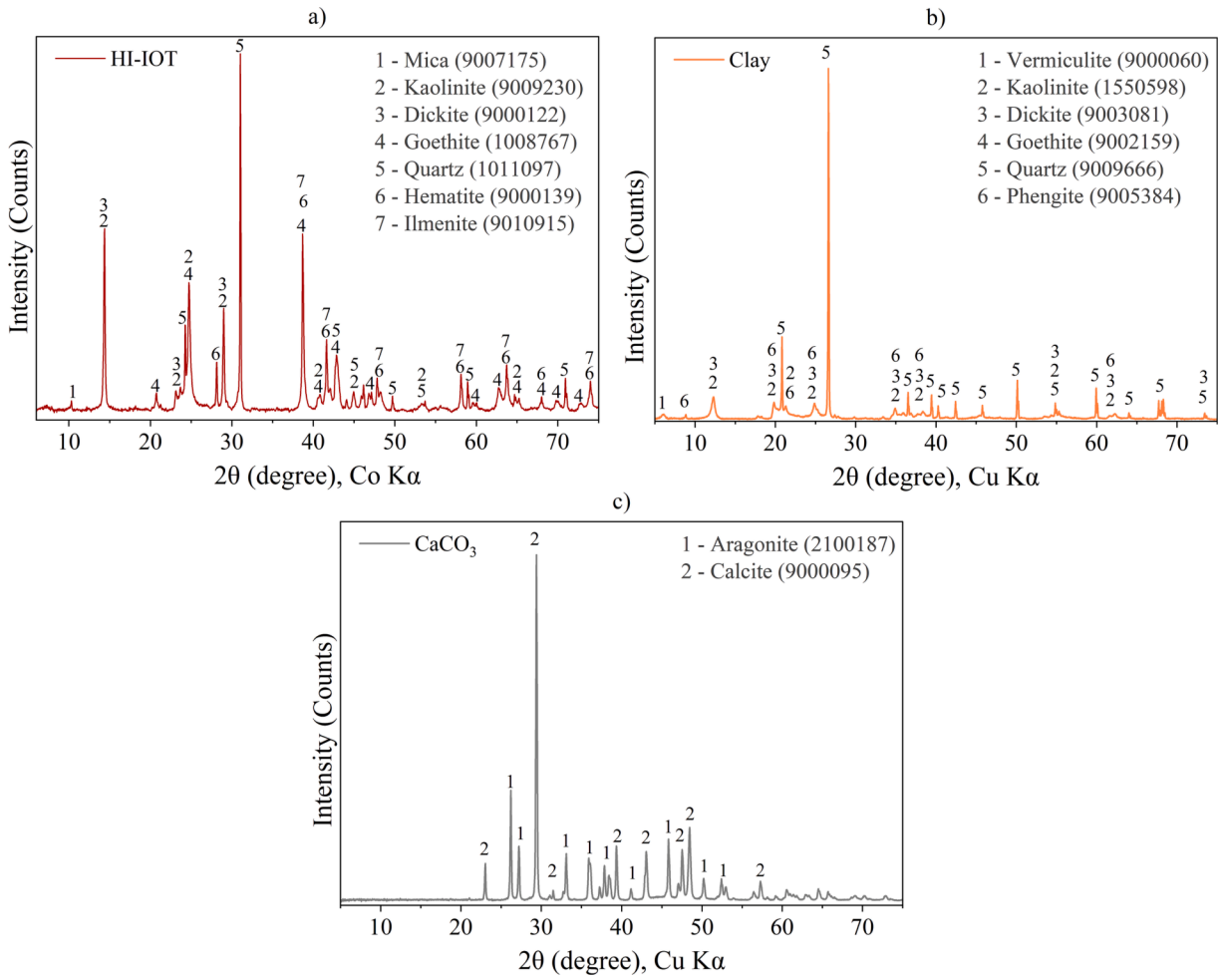

Fig. 1. X-ray diffraction patterns (5° – 75° 2θ range) of the raw materials: HI-IOT (a), clay (b), and $CaCO_3$ (c). COD database code in parentheses.

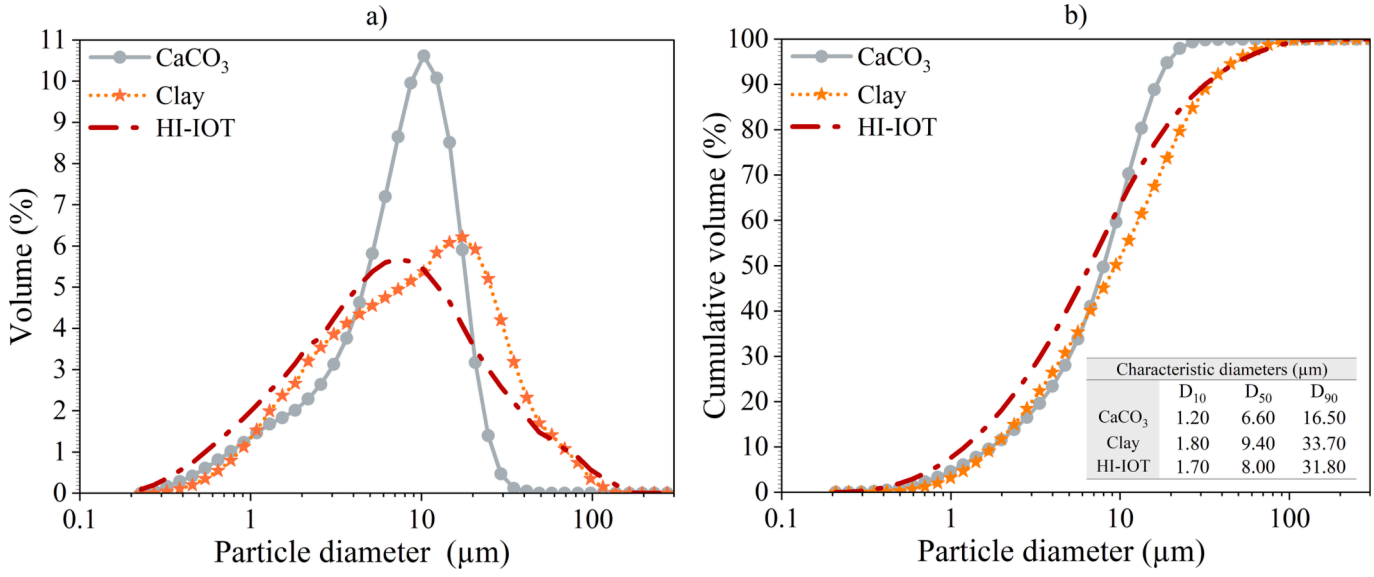

Fig. 2. Particle size distribution, volume (a) and cumulative volume (b).

of 1.7 to 2.4 [31]. The alite content was set to approximately 65%, which is a recommendation of industrial Portland clinker producers (Taylor,1997). The other moduli (SM and AM) maybe were changed with the incorporation of HI-IOT, as well as the expected content of other phases, such as belite, tricalcium aluminate, and ferrite. To simplify the discussion, tricalcium aluminate (C_3A) formed in clinker will be referred to as “aluminate” or "calcium aluminate".

The interstitial fraction (aluminate and ferrite phases) is the fraction

Table 2
Chemical moduli of the raw meals and the expected clinker phases.

Chemical moduli	HI-IOT content in the raw meal (%)					
	0	5	7.5	10	15	20
LSF	0.967	0.969	0.974	0.970	0.971	0.972
SM	2.79	1.97	1.69	1.48	1.16	0.94
AM	3.85	1.33	0.99	0.78	0.55	0.41
HM	2.27	2.11	2.05	1.97	1.84	1.72
Mineral phases (%)	HI-IOT content in raw meal (%)					
	0	5	7.5	10	15	20
Alite	65.1	65.2	66.2	65.3	65.2	65.2
Belite	14.9	11.3	8.66	7.85	4.61	1.32
Aluminate	14.0	8.41	5.59	2.86	−2.57	−7.95
Ferrite	5.01	14.0	18.5	23.0	31.7	40.4

Table 3
Samples identification and raw materials content.

Clinker	Aluminosilicates total (wt% in the raw meal)	HI-IOT (wt% in the raw meal)	Clay (wt% in the raw meal)	HI-IOT / Aluminosilicates total (wt%)	$CaCO_3$ (/wt% in the raw meal)
CI_0	21.96	0.00	21.96	0.00	78.04
CI_5	23.20	5.00	18.20	21.55	76.80
$CI_{7.5}$	23.75	7.50	16.25	31.58	76.25
CI_{10}	24.40	10.00	14.40	40.98	75.60
CI_{15}	25.70	15.00	10.70	58.37	74.30
CI_{20}	26.95	20.00	6.95	74.21	73.05

that most changes due to the increase in Fe_2O_3, which causes an increase in ferrite phase as well as a decrease in aluminate. In situations where the Al_2O_3/Fe_2O_3 (A/F) ratio is less than 0.64, C_3A formation is unlikely to occur in the absence of alumina to react with lime [24]. Thus, the HI-IOT content above 15 wt% shows negative C_3A content, and because of that, these contents were not considered to produce cement.

In general, the raw meal proportions, as given in Fig. 3, were kept close to the usual in Brazilian industry, i.e. approximately 80% of limestone and approximately 20% of the other raw materials compose of SiO_2, Al_2O_3, and Fe_2O_3. The samples CI_5, $CI_{7.5}$, and CI_{10} were selected for clinker production on a laboratory scale.

Due to the increase of Fe_2O_3 caused by HI-IOT incorporation, it's necessary to investigate its impact on the liquid phase (LP) or melt,

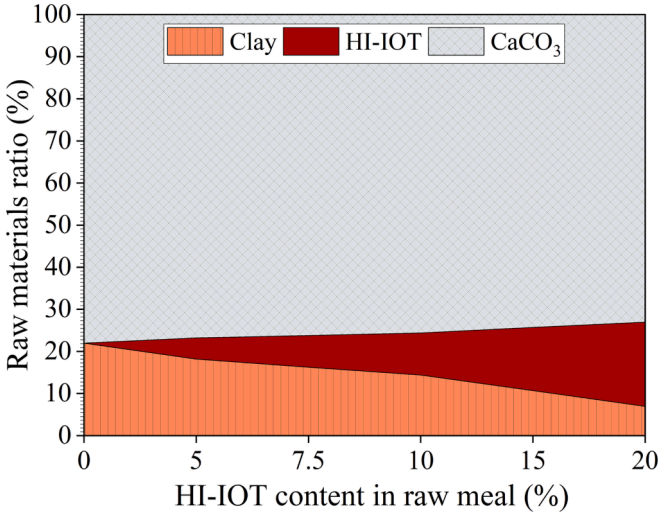

Fig. 3. Relationship between raw materials proportions and HI-IOT content in raw meal.

which appears at 1,338 °C, and it is believed to reach its maximum when AM = 1.38 [24]. The burning degree might be accelerated; the alite formation may be facilitated due to diffusion and transport by the liquid phase [24,32]. The LP was calculated at three different temperatures: 1,338 °C, 1,400 °C and 1,450 °C using the equations proposed by Lea and Parker [33] (**Eq. (1)** to **Eq. (4)**); where A = Al_2O_3 and F = Fe_2O_3.

$$LP_{1,338\ ^\circ C} = 6.10F + MgO + K_2O + Na_2O, \text{ if } AM \leq 1.38 \quad (1)$$

$$LP_{1,338\ ^\circ C} = 8.2\ A - 5.22F + MgO + K_2O + Na_2O, \text{ if } AM \leq 1.38 \quad (2)$$

$$LP_{1,400\ ^\circ C} = 2.95\ A + 2.20 \times F + MgO + K_2O + Na_2O \quad (3)$$

$$LP_{1,450\ ^\circ C} = 3.00\ A + 2.25 \times F + MgO + K_2O + Na_2O \quad (4)$$

2.3. Clinkerization procedures and characterization

The clay and HI-IOT were first oven-dried at 105 °C for 24 h. The mixture of the raw meal was homogenized in the Turbula System Schatz equipment for 5 min. The mixtures were rolled manually to produce spherical pellets of approximately 1 g ± 0.1 g with deionized water at a water/solid ratio of 0.60. The last process was dried in a furnace at 110 °C ± 5 °C for 24 h.

The clinkerization was carried out in a lab-scale static kiln EDG F1700 with a threshold at 1,200 °C and 1,500 °C with retention time of 30 min (selected from a Design of Experiments) in both temperatures, and a heating ramp at a speed of 15 °C/min. The pellets were supported in cobblestone-shaped magnesian refractories (4 cm × 5 cm × 7 cm) with a slightly hollow center. Then, a cooling process was realized using intense airflow on a metal plate (cooled with water recirculation). The quantity of mass needed for entire characterization at the laboratory was around 245 g (Figure S.1 - **Supplementary Data**).

The clinker grinding was set to maintaining 6 wt% of residues retained on the 75 μm sieve [34]. This process took place in two stages: a) Manual grinding: carried out in an agate mortar until the pellets are completely broken; b) Mechanical grinding: carried out in a planetary micro mill Pulverisette 7 – FRITSCH for 20 min at speed 9 (five spheres with a 1-cm radius).

The clinkers were physically characterized in terms of particle size distribution, specific gravity, and specific surface area. Particle size distribution was performed according to **section 2.1**. The specific gravity was determined by gas Helium (He) pycnometer in a Multi-pycnometer MVP 5DC, equipment of Quantachrome Instruments, from a simple average of 5 measurements. Specific surface area (SSA) was determined by BET [35] (SSA_{BET}) in Belsorp Max equipment, made by Bel Japan, through the physical adsorption of nitrogen gas at 77 K on the solid surface of the sample.

The mineralogical composition was quantitatively evaluated by QXRD. The XRD procedure was executed according to **section 2.1** as well as the Rietveld method. In the samples CI_0, CI_5 and $CI_{7.5}$ were detected most reactive crystalline structures of clinkers, such as monoclinic alite, β-belite, cubic aluminate and C_4AF as ferrite (Table S.6 - **Supplementary Data**).

2.4. Characterization of Portland cement pastes

2.4.1. Heat of hydration

The study used a composition of high early-strength Portland cement based on the Brazilian standard [34] to produce cement. The composition of the prepared Portland cement was 86.16% (g/g) of clinker, 3.84% (g/g) of calcium sulfate (G) ($CaSO_4{\cdot}2H_2O$, the content was optimized by calorimetry), and 10.0% (g/g) of $CaCO_3$ (C), representing filler content. Then, the Portland cement was named CI_5 - GC, $CI_{7.5}$ - GC, and CI_{10} – GC with 5, 7.5, and 10 wt% of HI-IOT in raw meal. As reference, a Brazilian high early strength Portland cement (H-OPC)

commercially available was used (specifications in Table S.7 - **Supplementary Data**), which is equivalent to a CEM I 42.5 R [36].

The cement pastes were produced with a water/cement ratio (w/c) of 0.5, using deionized water, to keep it according to cement standard tests, specifically concerning the Brazilian standard ABNT NBR 16697 [34] and European Standard EN 197–1: 2011 [36]. The materials were manually mixed for 30 s, followed by mechanical mixing of 60 s using an IKA stirrer with a rotational speed of 10,000 rpm [37]. The heat released was characterized by isothermal conduction calorimetry using I-CAL 8000 HPC (Calmetrix) with 8 channels. The analysis time was 48 h at 23 °C temperature.

2.4.2. Thermogravimetric analysis (TG/DTG)

To calculate the chemically combined water (C_w) and Portlandite content (CH) of hardened cement pastes over time, three cubic specimens molded for mechanical tests, and randomly selected, were summited to hydration stoppage by changing free water for organic solvents [38], such as isopropanol and diethyl ether. Thermogravimetric (TG/DTG) analyses were carried out after hydration stoppage. This test was performed in a thermobalance (NETZSCH, TG 209 F1 Libra) which around 50 mg of sample was placed in an open alumina crucible, where it was heated at a 10 °C/min rate until 1000 °C in inert (N_2) atmosphere (gas flow rate of 20 cm^3/min).

The quantity of portlandite was determined using the mass loss obtained for the tangential method by software Protheus Thermal analysis 8.0.2 (NETZSCH). For determining the hydration degree it was considered that all materials are full hydrated at 180 days [39]. Thus, C_w and CH are quantified as follows on **Eq. (5)** and **Eq. (6)** [28,40]:

$$C_w = \frac{W_{40} - W_{550}}{W_{550}} \tag{5}$$

$$CH = \frac{W_{410} - W_{550}}{W_{550}} \cdot \frac{M(Ca(OH)_2}{M(H_2O)} \tag{6}$$

where M is the molar mass, W_X is the percentage of mass loss at temperature × (in °C).

2.4.3. Mechanical properties

The mechanical properties (tensile strength, σ_t, and elastic modulus, E) of hardened cement pastes were determined using a method based on Point Load Test (PLT) method [41] to determine the tensile strength of the cement pastes (10-mm cubic size specimen). To determine elastic modulus, the PLT was instrumented with a LVDT (linear variable differential transformer) and used the Hertz Elastic Contact Theory (Hertz, 1882), and it has been named as PLT-LVDT [42,43]. To improve accuracy in measurements, the compression load was applied by semispheres of tungsten in quasi-static condition, with a load rate of 0.2 mm/min in two parallel faces (flat faces) of cubic samples. The assay was executed in a universal Instron machine (Model 5569) with a 50 kN load cell.

The cement pastes were molded with a fixed water to cement ratio (w/c = 0.5) in small cubic silicone molds (10-mm face; volume ~ 1000 mm^3). The fixed water to cement ratio was used to express the cement strength class according to the Brazilian standard ABNT NBR 16697 [34] and European Standard EN 197–1: 2011 [36] and to understand what commercial type of cement we can produce. At least 20 specimens were molded and vibrated on a vibration table for 60 s to reduce the occurrence of molding defects. During the first 24 h, the molds were kept in atmosphere with high internal relative humidity (RH > 90%). The PLT-LVDT test of cubes specimens (10 × 10 × 10 mm) was performed at 3, 7, 14, 28, and 104 (91 days only for CI_{10} - GC) days-age in a dry-surface saturated condition.

The tensile strength of cubes specimens (10 mm × 10 mm × 10 mm) was converted for compressive strength values of cylindrical specimens (27 mm × 54 mm) obtained by a Brazilian test (Figure S.2 - **Supplementary Data**). For the elastic modulus conversion, it used the following relation: $E_{cylindrical} = 6.68\ E_{PLT\text{-}LDVT}^{0.4339}$ (cylindrical with 27 × 54 mm) proposed by [44]. The cylindrical specimens' dimensions are smaller and tested in cement paste only when compared with the typical standard tests (done in a cylindrical of 50 × 100 mm dimensions and tested using standard sand with the cement); therefore, the results were converted and expressed as for the standard specimens.

2.4.4. Volumetric composition of hardened cement paste

The capillary porosity ($Porosity_{capillary}$) was calculated according to Powers's model [45] using the hydration degree and combined water obtained as described in **2.4.1**. **Eq. (7)** to **Eq. (13)** show the calculations used to determine the hydrated pastes capillary porosity.

$$V_{\text{capillary pores}} = V_{\text{paste}} - V_{\text{total solids}} \tag{7}$$

$$V_{\text{total solids}} = V_{\text{hydrated solids}} + V_{\text{anhydrous}} + V_{\text{gel water}} \tag{8}$$

$$V_{\text{hydrated solids}} = V_{\text{cement}} * DH_{\text{xdays}} + (Cw_{\text{xdays}} * 0.75) \tag{9}$$

$$V_{\text{gel water}} = V_{\text{hydrate solids}} * 0.389 \tag{10}$$

$$V_{\text{anhydrous}} = V_{\text{cement}} * (1 - DH_{\text{xdays}}) \tag{11}$$

$$Porosity_{\text{capillary}} = V_{\text{capillary pores}} / V_{\text{paste}} \tag{12}$$

$$CS = 0.254 * V_{\text{capillary pores}} \tag{13}$$

where DH_{xdays} is the degree of hydration in × days; Cw_{xdays} is the combined water in × days; $V_{hydrate\ solids}$ is volume of hydrates solids; $V_{gel\ water}$ is volume of gel water; $V_{anhydrous}$ is volume of anhydrous cement; $V_{capillary\ pores}$ is the volume of capillary pores; V_{cement} is volume of cement; CS is volume of chemical shrinkage.

The QXRD of hardened pastes was executed according to procedures shown in **section 2.1**. It was using the content of Portlandite, obtained as described in **2.4.2** as an internal standard. The final volumetric composition was calculated using the density of phases informed in the Cemdata18 database [46].

3. Results and discussion

3.1. Clinkers characterization

3.1.1. Chemical moduli and composition of clinkers

The chemical composition of clinkers was obtained experimentally (Table S.5 -**Supplementary Material**). After that, the chemical moduli were recalculated, as depicted in Fig. 4**a.** As planned, only the SM and AM exhibited significant variations**.** The addition of HI-IOT reduced the SM from 3.1 to 2.4, however, the values remained within the acceptable range for Portland clinker (2 to 3) [22]**.** The main alteration is the exponential decline in AM correlated with an increase in HI-IOT (Fig. 4**b**). This particular alteration has the considerable potential to impact clinker burnability [47].

The estimated liquid phase (LP) at high temperatures (Fig. 5**a**) content doesn't show significant variations. It stays in an optimal range of 20 to 30%. On the opposite, there are changes in LP content at its initial formation temperature (1,338 °C) due to AM reduction (Fig. 5**b**). The CI_5 and $CI_{7.5}$ display a proper quantity of LP (15 – 25%), and the CI_{10} seems have insufficient LP content [24,47].

3.1.2. XRD/QXRD

Fig. 6 presents the X-ray diffraction patterns scans of cement clinkers, and the angle regions of isolated phases are given in Fig. 7.

The diffraction band between 11.8° and 12.4° (2θ) (Fig. 7**a**) represents an isolated peak of C_4AF; its intensity increases in the function of the HI-IOT. Consequently, the aluminate peak intensity is reduced, as verified in the diffraction band between 32.9 ° and 33.6 ° (2θ) (Fig. 7**b**). The region between 30.7° and 31.4° (2θ) (Fig. 7**c**) corresponds to belite. A significant increase in the intensity of belite for CI_{10} is observed when compared to the other samples (CI_0, CI_5, and $CI_{7.5}$). The alite

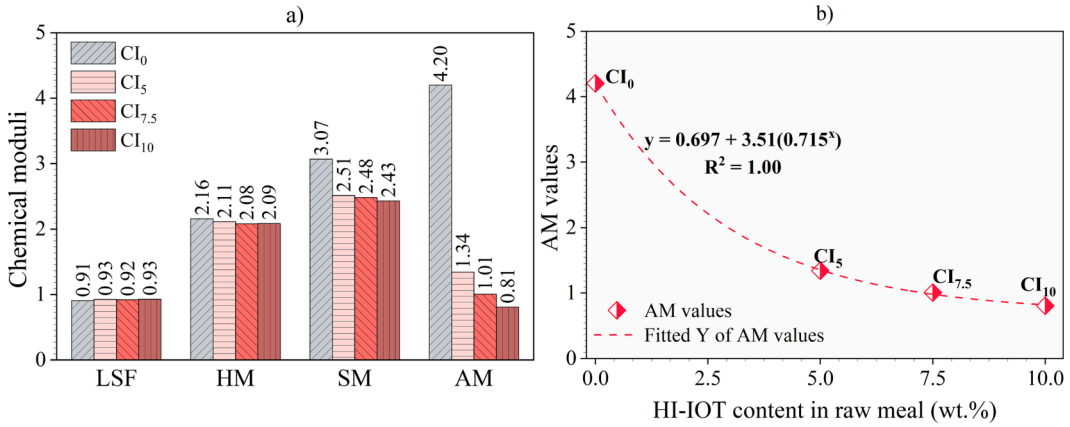

Fig. 4. Main chemical moduli of clinkers (a) and the relationship between AM and HI-IOT content in raw meal (b).

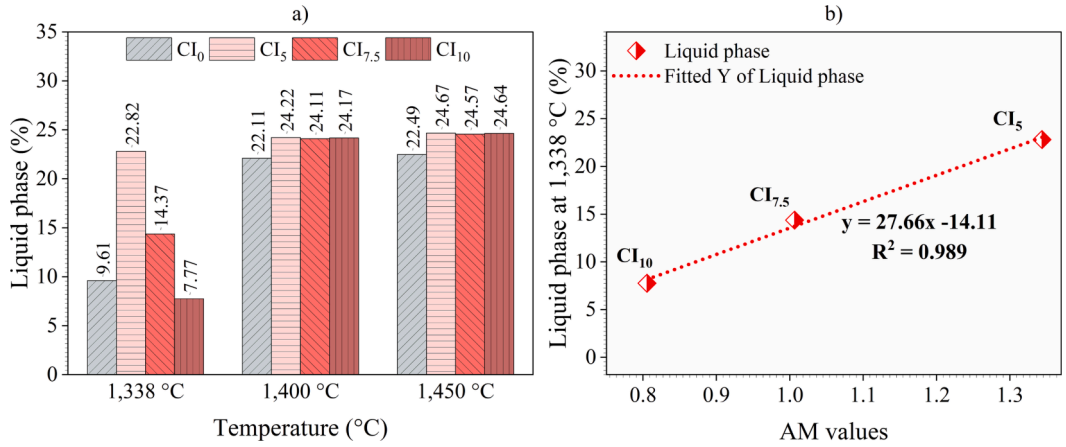

Fig. 5. Liquid phase content at different temperatures during the burning process (a) and their linear fit with AM content (below 1.38) (b).

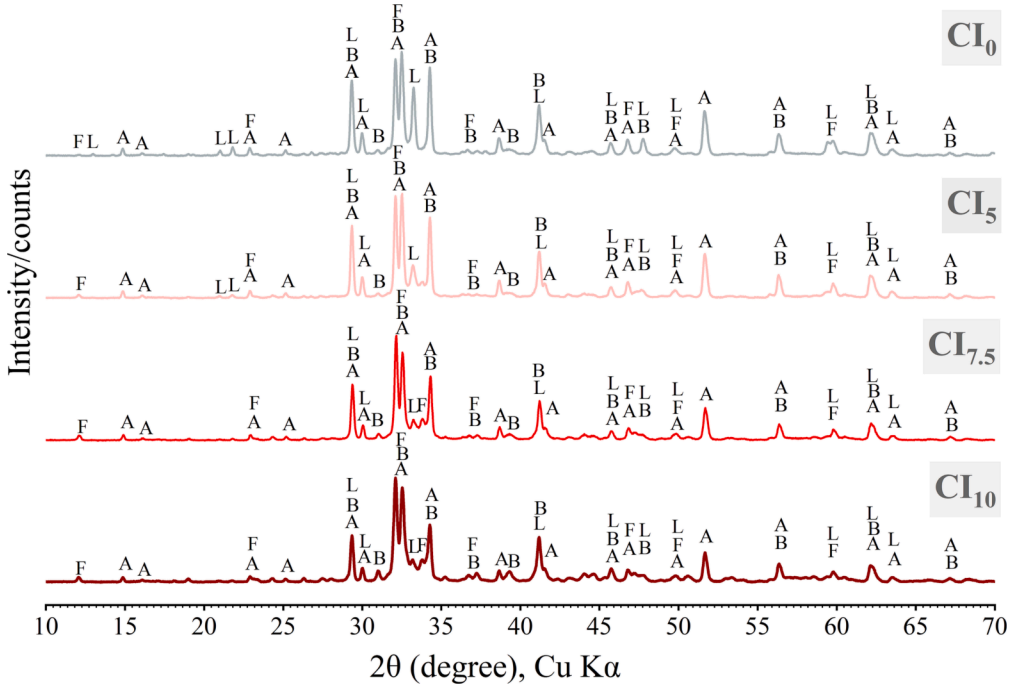

Fig. 6. X-ray diffraction patterns scans (10° – 70° 2θ range) of cement clinkers normalized by dividing maximum intensity. Alite (A), Belite (B), Ferrite (F) and Aluminate (L).

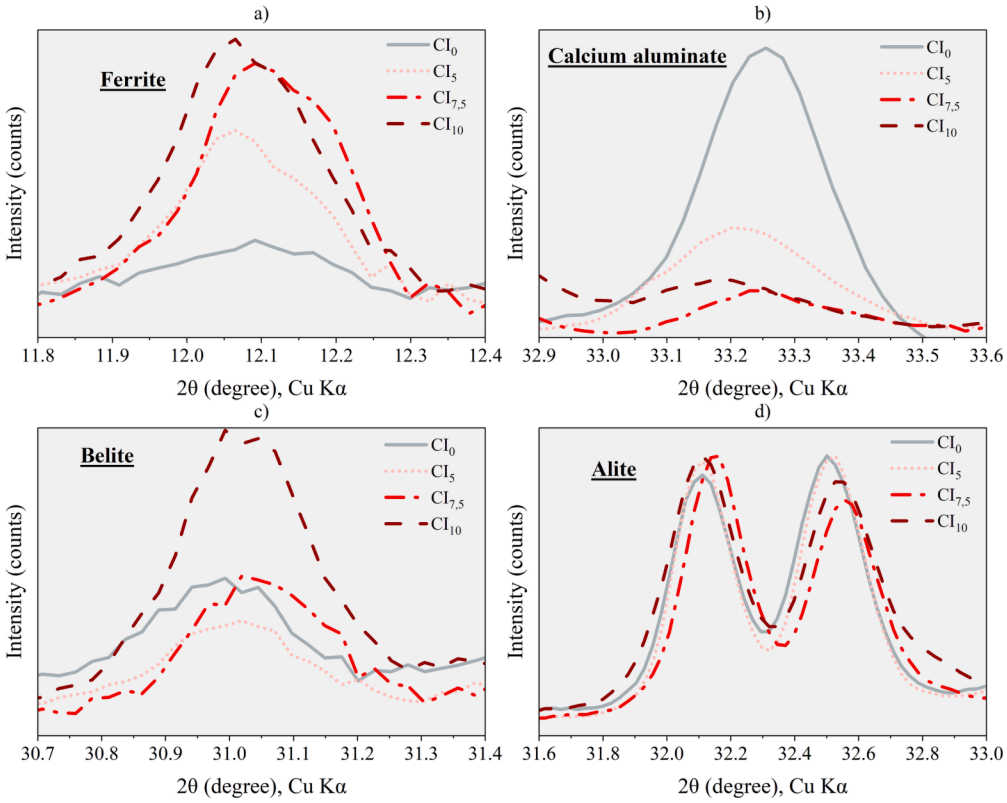

Fig. 7. Specific angular range of the XRD scans for clinker minerals, such as ferrite (a), calcium aluminate (b), belite (c) and, alite (d).

polymorphs present in range 31.6° and 33° (2θ) (Fig. 7**d**) are monoclinic types (M1 and M3), as expected for clinker Portland [48].

The results of the QXRD analysis are presented in Fig. 8. Indices of Rietveld refinement are given in (Table S.6 - **Supplementary Material**). The alite content (Fig. 8**a**) is appropriate for clinker Portland CI_0, CI_5, and $CI_{7.5}$, which are accompanied by a reduction in the belite phase that contradicts Bogue's predictions (Table 2). The samples with reduced liquid phase may fall outside the scope of the Bogue calculation, as it's not designed to account for such conditions [21].

Fig. 8**b** shows the interstitial phase contents (aluminate; ferrite). Concerning the limits, all samples with HI-IOT resulted in higher C_4AF content and lower C_3A content [22] for a Portland cement clinker; typically 8% and 10%, respectively. However, 10% of HI-IOT in "raw meal" significantly impacted the liquid phase content at 1,338 °C (Fig. 5**a**), hindering the formation of alite. The AM above 1.0 (LP above 14% at 1,338 °C) is enough for alite formation in ideal content (~60%).

Table 4 exhibits the summary of QXRD. The HI-IOT incorporation doesn't significantly change the total quantity of silicates and interstitial fractions. Specifically, this addition reduced the alite/belite ratio by up to 75%, while the ferrite/aluminate ratio increased to nearly 70%.

Table 4
Mineralogical summary of QXRD results.

Sample	Silicates fraction[1]	Interstitial Fraction[2]	Alite/Belite ratio	Ferrite/Aluminate ratio
CI_0	85.0	15.0	2.95	0.12
CI_5	81.1	17.5	4.88	2.57
$CI_{7.5}$	81.7	16.8	2.60	4.42
CI_{10}	80.2	18.9	1.22	8.45

[1] Silicates fraction = sum of alite and belite; [2]Interstitial fraction = sum of ferrite and aluminate.

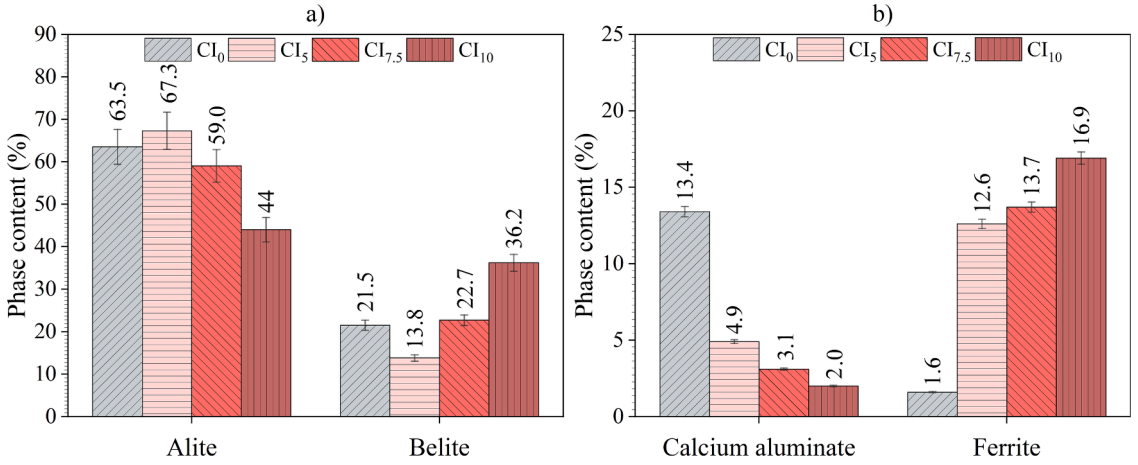

Fig. 8. QXRD results for silicates phases (a) and interstitial phases (b) for cement clinkers. Uncertainties from Robin round [49].

Microstructure of clinkers were analyzed by optical microscopy (see Supplementary Material, and Table S.5 to S.7). All clinkers exhibit proper crystals dimensions of belite (20 to 40 μm; type I) and alite (20——33 μm) [48] and similar porosity range of 20–30%. The edges of the alite were observed to be free from decomposition.

3.1.3. Physical characterization

Fig. 9 presents the particle size distributions of the clinkers. Table 5 provides the statistical parameters of the particle size distribution, as well as other physical properties such as specific surface area and specific gravity. The results show slight differences in the physical characteristics of the samples.

The specific gravity of CI_0 is lower than the others because this sample has a higher alite content (Specific gravity of 3.04 g/cm^3, the lowest among clinker minerals). While in the other ones, the density increased in the function of the ferrite content increased (specific gravity of 3.77 g/cm^3, the highest among clinker minerals).

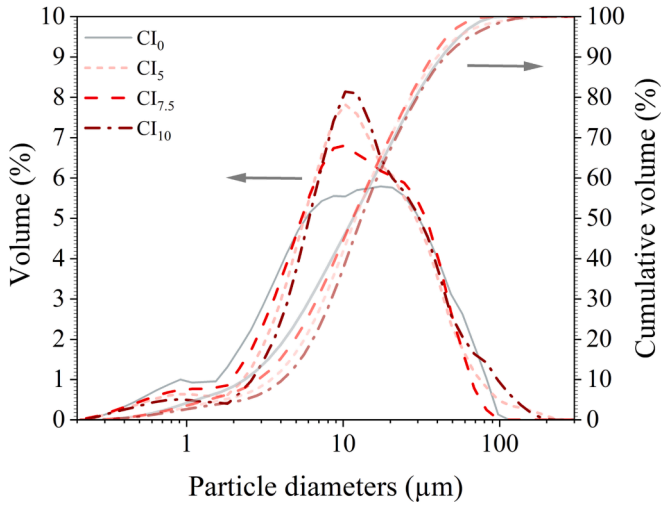

Fig. 9. Particle size distribution of clinkers.

Table 5
The physical properties of Portland clinkers.

Samples	SSA_{BET} (m^2/g)	Specific gravity (g/cm^3)	Characteristics diameters (μm)		
			D_{10}	D_{50}	D_{90}
CI_0	0.736	3.19 ± 0.008	2.4	11.6	42.8
CI_5	0.688	3.22 ± 0.001	3.5	12.1	40.0
$CI_{7.5}$	0.711	3.24 ± 0.005	2.9	11.5	37.0
CI_{10}	0.781	3.27 ± 0.010	4.1	13.1	44.7

3.2. Characterization of Portland cement pastes

3.2.1. Heat of hydration, setting time estimation

Fig. 10 shows the mineralogical mass composition of cement. The ferrite content of Portland cement varied from 11 to 15 wt% inside the values for ordinary Portland cement (OPC) [50]. The lower C_3A values allow for classifying the cement analyzed in this work as sulfate-resisting Portland cement, CEM I-SR [36].

Table 6 and Fig. 11**a** show the curves of the heat flow and cumulative heat curves during 48 h of hydration for Portland cement pastes. The resemblant particle size distribution of clinkers (Fig. 9) indicates that this factor doesn't interfere with the heat generation rate of the cement prepared in this study.

Due to the reduction of aluminate maintaining the same calcium sulfate content in samples with HI-IOT, there is an increase in the

Table 6
Characteristics of early hydration time.

Samples	Reaction rate (mW/g. h)	Maximum peak (mW/g)	Setting time by ASTM C1679-13 (h:min)	Induction period (h:min)	Total cumulative heat by 72 h (J/g)*
CI_5 - GC	1.05	5.31	04:35	01:15	254.1 ± 4.8
$CI_{7.5}$ - GC	1.03	4.46	04:20	01:20	244.9 ± 4.8
CI_{10} - GC	1.32	3.93	04:30	01:15	235.7 ± 4.8
H - OPC	1.06	3.81	05:30	01:50	224.4 ± 4.8

* Repeatability standard deviation (within laboratory) by robin round test [53].

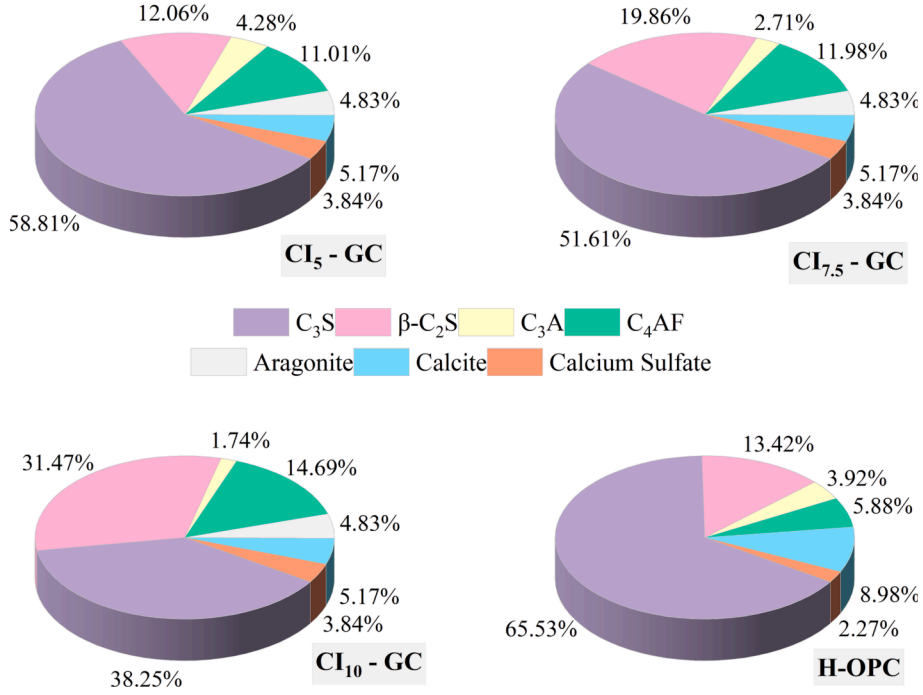

Fig. 10. Mass composition of anhydrous cements.

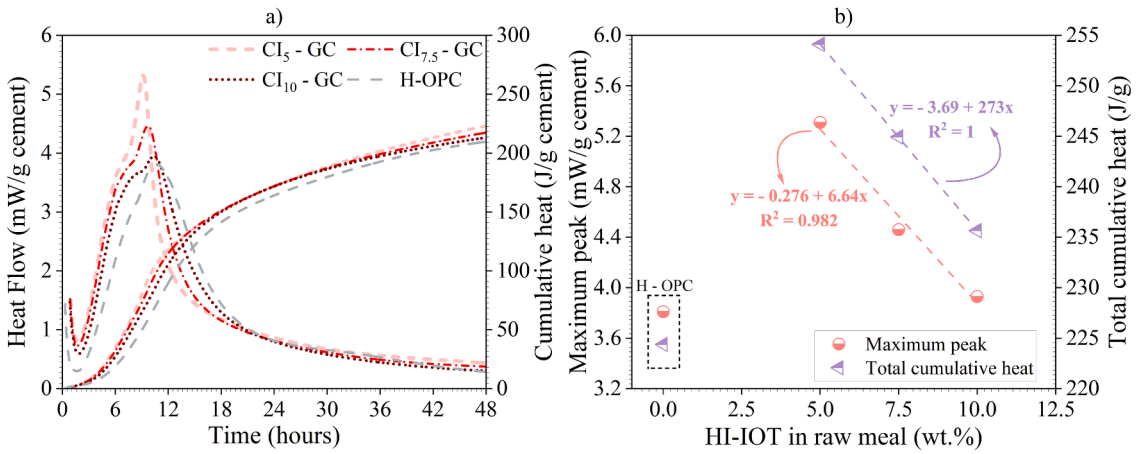

Fig. 11. Heat released curves (a) and their relationship with HI-IOT content (Dash lines are fitted for y axis) (b).

gypsum/C_3A ratio from 0.90 to 2.20 between 5 and 10 wt% of HI-IOT, respectively. Then, it leads to C_3A hydration retard in the sequence CI_{10} – GC > $CI_{7.5}$ – GC > CI_5 – GC [51], as given in the heat flow profile between 7 and 14 h. Furthermore, the heat released data indicate a reduction in the maximum peak when HI-IOT was incorporated, as well as the total cumulative heat (Fig. 11**b**). This can be attributed to the reduction of more reactive phases, such as alite and C_3A [52].

3.2.2. *Monitoring hydration using TG/DTG*

Fig. 12**a** displays the amount of CH that has been formed. The CI_{10} - CG exhibits the lowest CH values, which can be attributed to its lower alite content (44 % g/g) (Fig. 8). In contrast, the H-OPC presents 7 to 14% more alite than the other samples (CI_5 – GC and $CI_{7.5}$ -GC). For this reason, its CH content is highest. These variations in CH precipitation can be attributed to several factors besides the alite content, such as belite content, alite solubility, and microstructure [52,54].

The H-OPC sample exhibits a higher reactivity during the initial ages (Fig. 12**b**), as expected for the Brazilian high initial strength Portland cement. The combined water is within 20 – 28 wt% in the analyzed period. While the other samples hardly exceed 23 wt% in the same period. Although H-OPC has higher combined water, the hydration degree (HD) has slightly higher values in the initial ages only, then they are equal or even have a lower hydration degree than the other samples (Fig. 12**c**). The higher belite content (36 % g/g) in the CI_{10} – CG caused

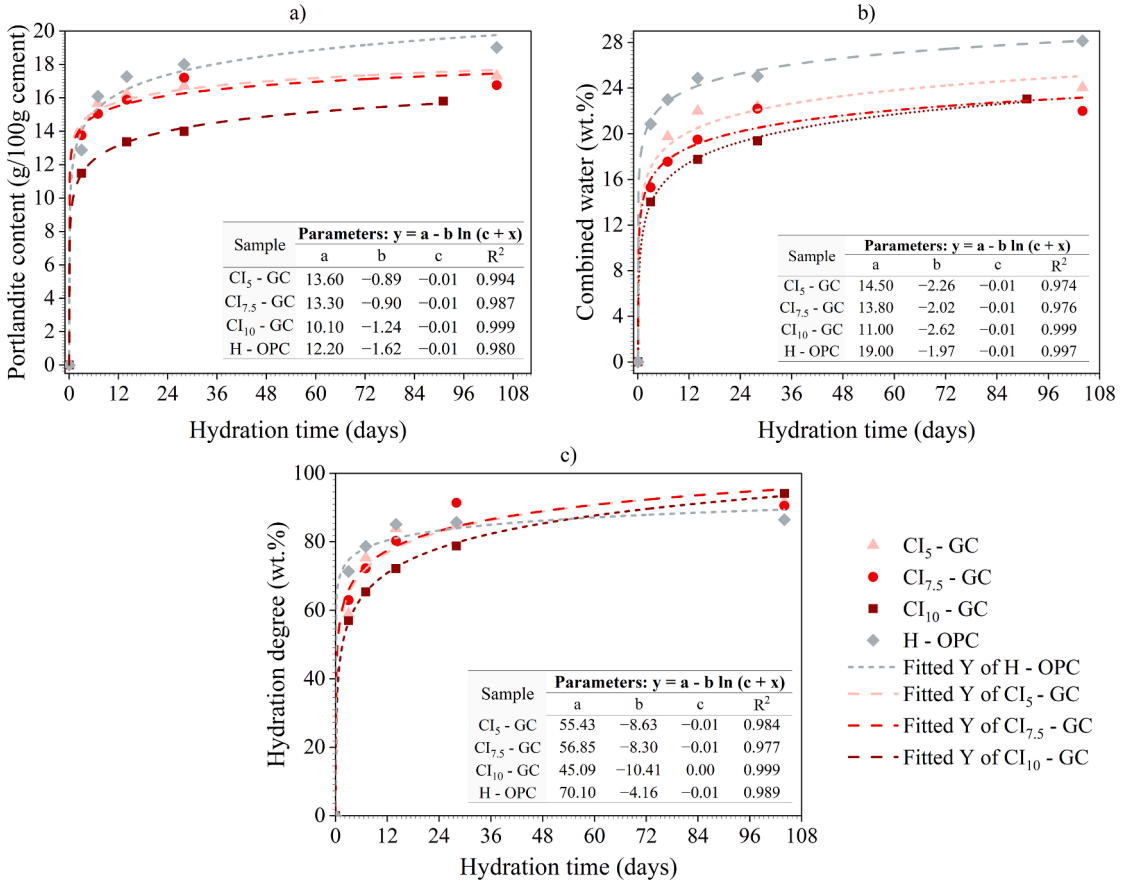

Fig. 12. Amount of portlandite (a), combined water (b) and hydration degree. Single caption. HD for CI_{10} – GC at 104 days was estimated by logarithm fit.

an increase in reactivity at advanced ages because the C_2S component dissolves more slowly than the C_3S component [52].

3.2.3. Mechanical properties by reduced size test

Fig. 13 presents the mechanical properties of the samples. It shows a high correlation with hydration behavior (Fig. 14**a and b**). The H-OPC in the initial 28-day period demonstrates a high evolution of the compressive strength that subsequently reduced and stabilized over time (Fig. 13**a**). Conversely, the other samples exhibit an initially slower rate of compressive strength development, but their mean values surpass that of H-OPC after 28 days.

About elastic moduli results (Fig. 13b), slightly differences were observed when clinker incorporated HI-IOT in relation to the H-OPC (reference); particularly, before the 28-days of age. The difference increased with the increase of HI-IOT replacement in the clinker Portland cement. After the 28-day of age, 5% of HI-IOT replacement resulted in the highest elastic moduli, superior of the H-OPC (reference), and no more differences of elastic modulus for 7.5 and 10% of HI-IOT replacement in clinker Portland, in comparison with the reference; H-OPC. The elastic modulus results followed a similar tendency of those observed for compressive strengths, but the differences observed are reduced. Specifically, the elastic modulus at 28-days age yielded values of 12.33–13.17 GPa, within the expected range for a cement (10 – 30 GPa) [55].

The differences in compressive strength among the samples can be attributed to several factors. In this study, the hydration of silicate phases has a strong influence on strength development. The samples with higher alite content show higher compressive strength values in the early stages (up to 28 days), while the progressive increase at advanced age in compressive strength is primarily due to belite content [56,57].

Under the conditions tested, up to 7.5% (g/g) of HI-IOT can be incorporated in "raw meal" to produce Portland cement with similar reactivities to that observed for the H-OPC. 10 % g/g of HI-IOT impaired the cement paste strength due to reduced alite content (Fig. 8). Thus, these results classified the samples CI_5 – GC and $CI_{7.5}$ – GC as CEM I 42.5 R, and the CI_{10} – GC is more suitable for CEM I 32.5 R according to

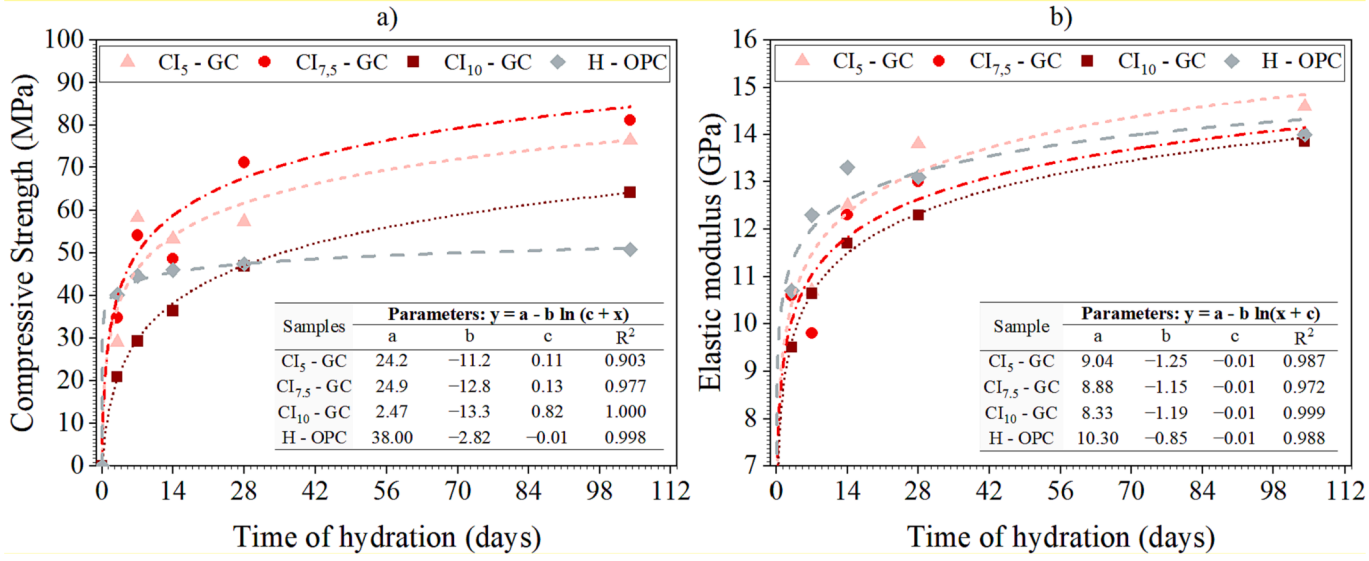

Fig. 13. Evolution over time of mean tensile strength (a) and mean elastic modulus (b). Lines represent the fitted curves. Results for CI_{10} – GC at 104 days were estimated by logarithm fit.

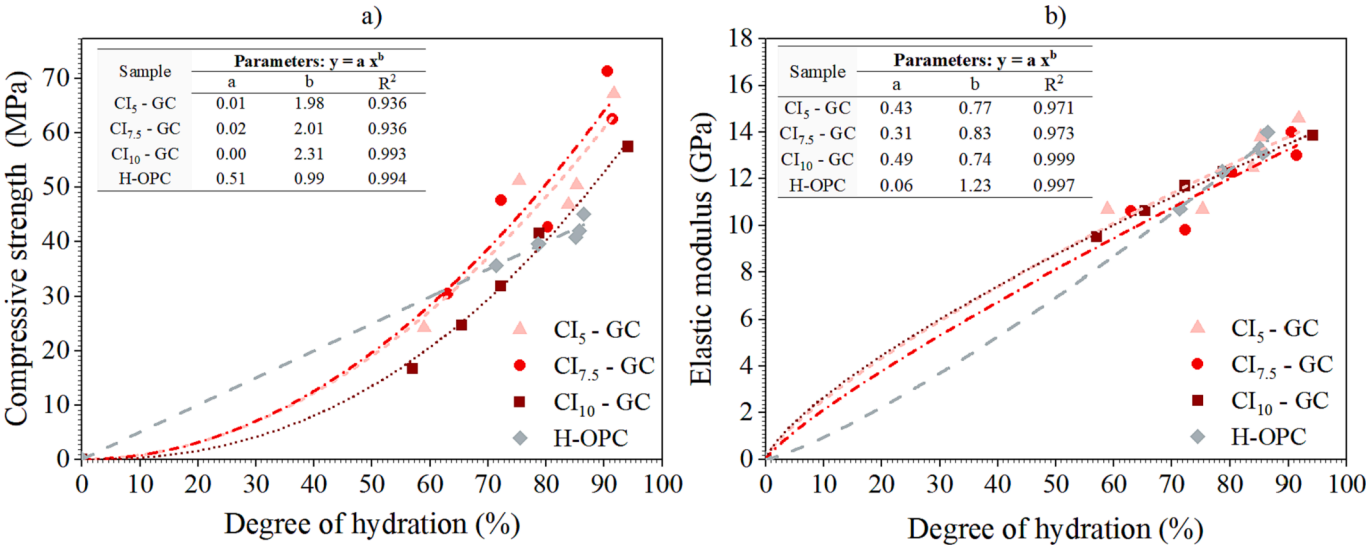

Fig. 14. Correlations between the average mechanical properties, tensile strength (a) and elastic modulus (b) and the degree of hydration.

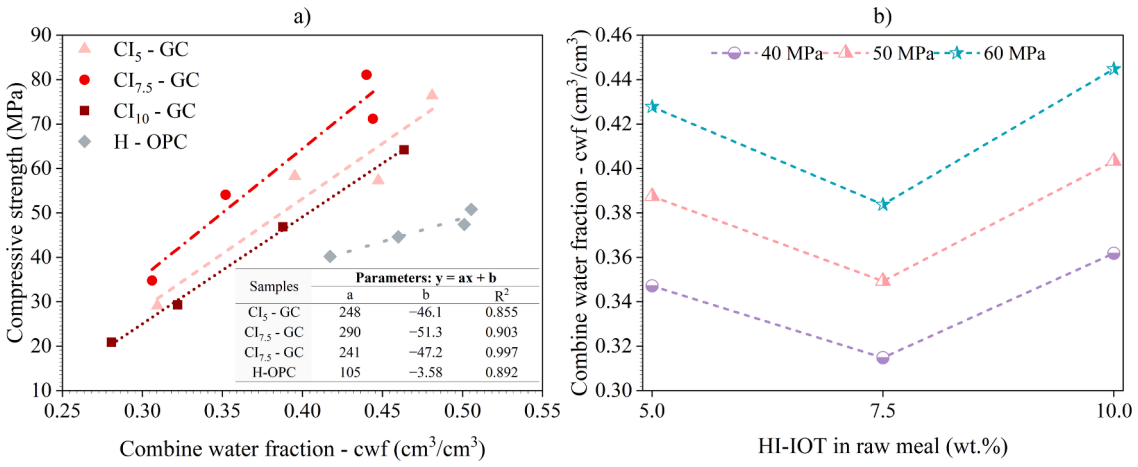

Fig. 15. Combine water fraction versus compressive strength (a) and their relationship with HI-IOT content in raw meal for 40, 50 and 60 MPa (b).

European standards [36].

The compressive strengths for the 7.5% (g/g) of HI-IOT achieved 34.80 MPa (3 days-age), 54.10 MPa (7 days-age), and 71.20 MPa (28 days-age). All compressive strength results were superior to the minimum required by Brazilian standard ABNT NBR 16697 [34] and European Standard EN 197–1: 2011 [36] for commercial cement specifications, including the high-initial strength ones [34]. Both standards use water to cement ratio of 0.5 to produce the cement pastes. Once the use of water reducing agent is crucial for the cement applicability, we recommend to overcome the limitations of our investigation simulating reduced and other water-to-cement ratios, as done by Oliveira et al. [42].

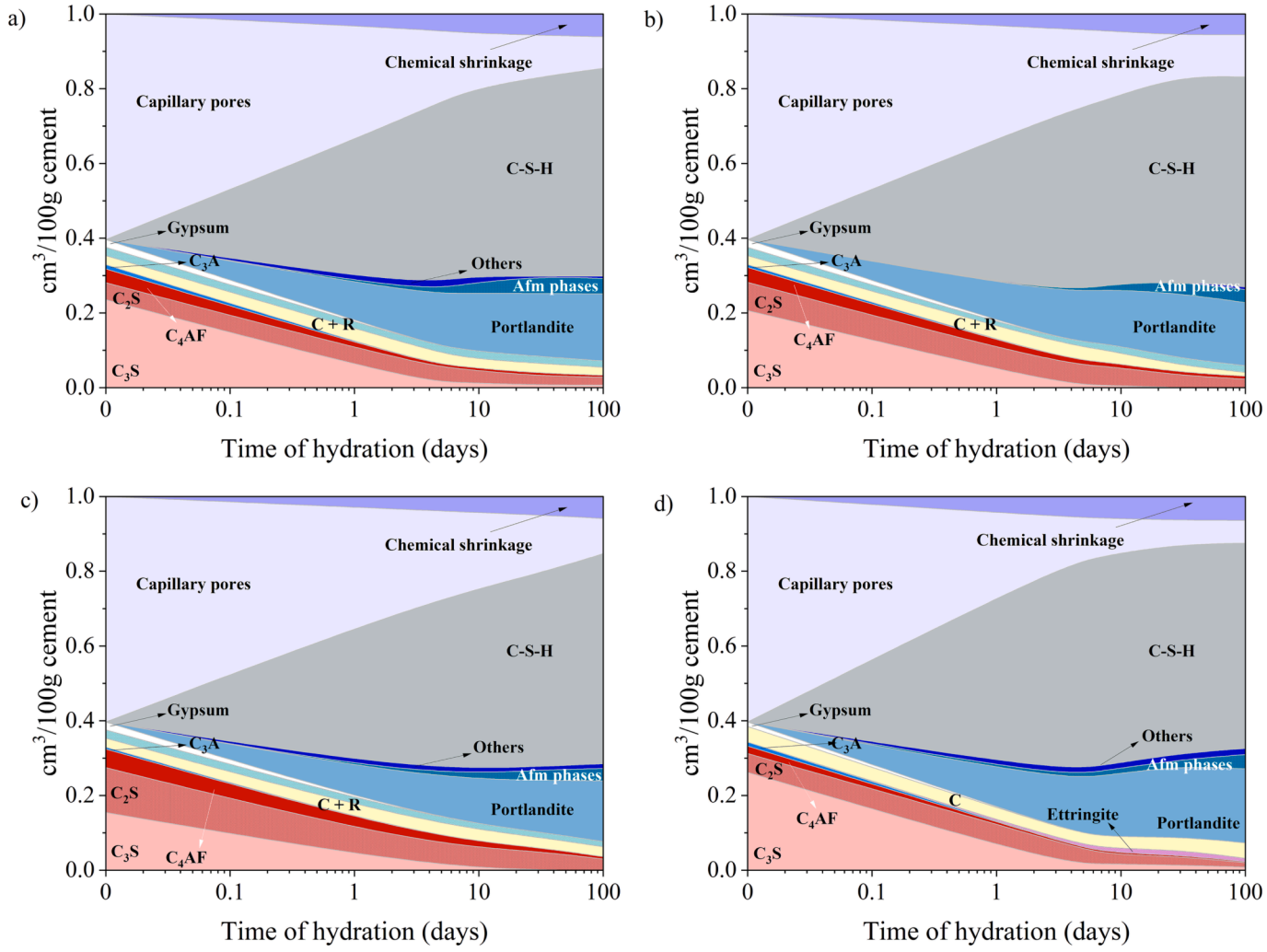

Fig. 16. Volumetric composition of cement pastes over time for CI_5-GC (a), $CI_{7.5}$ – GC (b), CI_{10} – GC (c) and H-OPC (d). Calcite (C) and Aragonite (R). Phase quantification by QXRD (Table S.8 and Table S.9 - Supplementary Material).

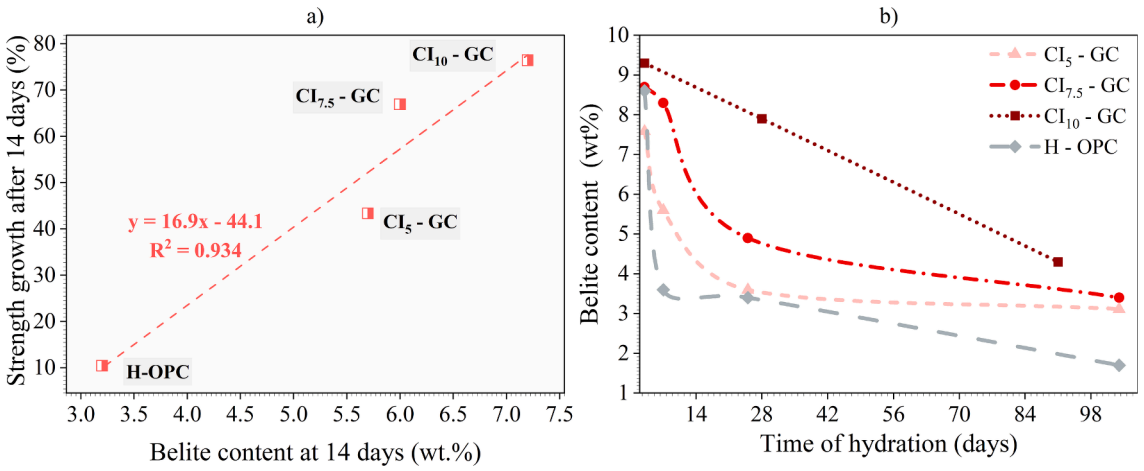

Fig. 17. Correlation for the increase (%) of compressive strength between 14 and –104 days and the content of belite at 14 days by QXRD (a). Belite content over time (b).

Fig. 15 illustrates the correlation between compressive strength and the combined water fraction (cwf) [39] for cement pastes. The findings indicate that distinct cwf values may be required for the same compressive strength (Fig. 15**a**), and the $CI_{7,5}$ – GC requires less combined water consumption while maintaining the same strength class (Fig. 15**b**). Consequently, factors apart from combined water fraction, such as porosity and mineral phase hydration, can govern these mechanical strength outcomes.

3.2.4. Evolution of the volumetric composition of the cement paste

Fig. 16 shows the volumetric composition diagrams of cement pastes over time. The samples displayed the hydrates for limestone cement [58]. Ettringite is more prominent at three days and nearly absent before that (Figure S.3 – **Supplementary Material**). The monocarboaluminate was the main Afm phase formed from the reaction of $CaCO_3$ with C_3A and/or C_4AF [59]. Due to the low aluminum content in the samples, Fe-monocarbonate was presumably forming as well [46,60].

The expected product of ferrite hydration is the Fe-siliceous hydrogarnet. However, its detection using XRD require more treatment since the first peak of this phase is located near a CH peak ($2\theta \sim 17.47°$) [46]. Thus, the ferrite hydrate wasn't incorporated into the volumetric composition.

The hydration of silicate phases resulted in C-S-H and Portlandite formation [56]. The C-S-H formed is the most significant difference among the samples (Fig. 16). The H-OPC sample shows stabilization in C-S-H formation around ten days of hydration, whereas the CI_{10}-GC sample has continued to increase its C-S-H content without stabilization. This circumstance may be attributed to the lower amount of silicate anhydrous present in H-OPC before ten days of hydration and their high reactivity in early ages.

Thus, the most notable disparity resulting in hardened cement pastes behavior is the anhydrous phase content, mainly in belite phase, as given in Fig. 17**b**. Consequently, the anhydrous phase represents a crucial mechanism for assessing the mechanical strength of hardened cement pastes (Fig. 17**a**), mainly in advanced ages, in addition to porosity and degree of hydration.

4. Conclusions

The lab-scale test approach used herein was potentially relevant to find the correlations between chemical, physical, mineralogical, and mechanical properties obtained in the study and an accurate assessment of the optimal conditions for using these tailings as an alternative raw material in clinker production. All results were obtained in a laboratory using reduced-sized scale tests, but it was enough to clarify the reactiveness and strength evolution potential for the industrial scale application.

The substitution of clay by Brazilian iron ore tailing with mainly iron oxide contents is promising up to 7.5 wt% in the clinker raw meal, and it was suitable for producing a Brazilian high initial strength Portland cement. It obtained compressive strength results of 34.8 MPa, 54.10 MPa and 71.20 MPa at 3 days, 7 days and 28 days-age, respectively. Besides that, up to 10 wt% in the clinker raw meal can produce Portland cement with 32 MPa strength class and possibly sulfate-resistant cement. This kind of cement shows improvement in mechanical strength after 90 days, compatible with the construction of dams and other types of infrastructure construction sites.

CRediT authorship contribution statement

Natacha C. N. Faria: Writing – original draft, Methodology, Investigation, Formal analysis, Conceptualization. **Valdir M. Pereira:** Writing – review & editing, Formal analysis. **Thiago R. S. Nobre:** Methodology, Investigation, Formal analysis, Conceptualization. **Roberto Cesar de O. Romano:** . **Antonio C. Vieira Coelho:** . **Sergio C. Angulo:** Writing – review & editing, Supervision, Project administration, Methodology, Investigation, Funding acquisition, Formal analysis, Conceptualization.

Declaration of Competing Interest

The authors declare that they have no known competing financial interests or personal relationships that could have appeared to influence the work reported in this paper.

Data availability

Data will be made available on request.

Acknowledgments

This research was funded by VALE SA company, in the scope of EMBRAPII Sustainable Construction Unit CICS-USP. The authors also thank the research infrastructure support provided by the National Institute of Science and Technology "Advanced Eco-Efficient Cement-Based Technologies", between USP and CNPq agency. Sérgio C. Angulo received the research scholarship grant from CNPq process number 307458/2021-0. The author expresses gratitude to Mateus Zanovello, a master's student, for providing Portland cement (reference) raw data from his research, and to Pedro R. Alves Abrão, a PhD student of the

group, for contributing with their knowledge of using cwf indicator, based on combined water and porosity formation of the cement pastes.

We recognized Dra. Maria Alba Cincotto as a co-author and supervisor of this research. She unfortunately passed away and she cannot be added as a co-author. She was a scientist leader of Cement Chemistry in Brazil, and our group wants to recognize her scientific contributions in our context and in this manuscript. Thanks to the partnership of many years, the transmission of all scientific concepts and values.

Appendix A. Supplementary data

Supplementary data to this article can be found online at https://doi.org/10.1016/j.conbuildmat.2023.132958.

References

[1] D. Siqueira, R. Cesar, R. Lourenço, A. Salomão, M. Marques, H. Polivanov, M. Teixeira, M. Vezzone, D. Santos, G. Koifman, Y. Fernandes, A.P. Rodrigues, K. Alexandre, M. Carneiro, L.C. Bertolino, N. Fernandes, L. Domingos, Z. C. Castilhos, Terrestrial and aquatic ecotoxicity of iron ore tailings after the failure of VALE S.A mining dam in Brumadinho (Brazil), J. Geochem. Explor. 235 (2022), 106954, https://doi.org/10.1016/j.gexplo.2022.106954.

[2] L.H. Silva Rotta, E. Alcântara, E. Park, R.G. Negri, Y.N. Lin, N. Bernardo, T.S. G. Mendes, C.R. Souza Filho, The 2019 Brumadinho tailings dam collapse: Possible cause and impacts of the worst human and environmental disaster in Brazil, Int. J. Appl. Earth Obs. Geoinformation. 90 (2020) (2019), 102119, https://doi.org/10.1016/j.jag.2020.102119.

[3] R. Sapata Gonzalez, R. Aparecida da Silveira Rossi, L. Gustavo Martins Vieira, Economic and financial consequences of process accidents in Brazil: multiple case studies, Eng. Fail. Anal. 132 (2022), 105934, https://doi.org/10.1016/j.engfailanal.2021.105934.

[4] P. Kinnunen, M. Karhu, E. Yli-Rantala, P. Kivikytö-Reponen, J. Mäkinen, A review of circular economy strategies for mine tailings, Clean. Eng. Technol. 8 (2022), 100499, https://doi.org/10.1016/j.clet.2022.100499.

[5] J. Kirchherr, D. Reike, M. Hekkert, Conceptualizing the circular economy: an analysis of 114 definitions, Resour. Conserv. Recycl. 127 (2017) 221–232, https://doi.org/10.1016/j.resconrec.2017.09.005.

[6] A. Aranda Usón, A.M. López-Sabirón, G. Ferreira, E. Llera Sastresa, Uses of alternative fuels and raw materials in the cement industry as sustainable waste management options, Renew. Sustain. Energy Rev. 23 (2013) 242–260, https://doi.org/10.1016/j.rser.2013.02.024.

[7] K.A. Clavier, J.M. Paris, C.C. Ferraro, E.T. Bueno, C.M. Tibbetts, T.G. Townsend, Washed waste incineration bottom ash as a raw ingredient in cement production: Implications for lab-scale clinker behavior, Resour. Conserv. Recycl. 169 (2021), 105513, https://doi.org/10.1016/j.resconrec.2021.105513.

[8] L. Žibret, A. Ipavec, S. Dolenec, Microstructural characteristics of belite–sulfoaluminate cement clinkers with bottom ash, Constr. Build. Mater. 321 (2022), 126289, https://doi.org/10.1016/j.conbuildmat.2021.126289.

[9] Y. Liu, C. Yang, F. Wang, S. Hu, M. Zhu, C. Hu, L. Lu, Z. Liu, Evaluation on recycled clinker production and properties from regeneration of completely recycle concrete, Constr. Build. Mater. 301 (2021), 123882, https://doi.org/10.1016/j.conbuildmat.2021.123882.

[10] S. Jian, W. Gao, Y. Lv, H. Tan, X. Li, B. Li, W. Huang, Potential utilization of copper tailings in the preparation of low heat cement clinker, Constr. Build. Mater. 252 (2020), 119130, https://doi.org/10.1016/j.conbuildmat.2020.119130.

[11] Y. Wang, T. Zhang, Y. Zhang, G. Lyu, W. Zhang, Mineral transformation in treating low-grade bauxite using the calcification–carbonization process and preparing cement clinker with the obtained residue, Miner. Eng. 138 (2019) 139–147, https://doi.org/10.1016/j.mineng.2019.04.031.

[12] Y. Da, T. He, C. Shi, M. Wang, Y. Feng, Potential of preparing cement clinker by adding the fluorine-containing sludge into raw meal, J. Hazard. Mater. 403 (2021), 123692, https://doi.org/10.1016/j.jhazmat.2020.123692.

[13] N. Zhang, B. Tang, X. Liu, Cementitious activity of iron ore tailing and its utilization in cementitious materials, bricks and concrete, Constr. Build. Mater. 288 (2021), 123022, https://doi.org/10.1016/j.conbuildmat.2021.123022.

[14] K.D.C. e S. Defáveri, L.F. dos Santos, J.M. Franco de Carvalho, R.A.F. Peixoto, G. J. Brigolini, Iron ore tailing-based geopolymer containing glass wool residue: A study of mechanical and microstructural properties, Constr. Build. Mater. 220 (2019) 375–385, https://doi.org/10.1016/j.conbuildmat.2019.05.181.

[15] L.F.d. Magalhães, S. França, M.D.S. Oliveira, R.A.F. Peixoto, S.A.L. Bessa, A.C.d. S. Bezerra, Iron ore tailings as a supplementary cementitious material in the production of pigmented cements, J. Clean. Prod. 274 (2020), 123260, https://doi.org/10.1016/j.jclepro.2020.123260.

[16] B.C. Mendes, L.G. Pedroti, M.P.F. Fontes, J.C.L. Ribeiro, C.M.F. Vieira, A. A. Pacheco, A.R.G. de Azevedo, Technical and environmental assessment of the incorporation of iron ore tailings in construction clay bricks, Constr. Build. Mater. 227 (2019), 116669, https://doi.org/10.1016/j.conbuildmat.2019.08.050.

[17] L. Luo, Y. Zhang, S. Bao, T. Chen, Utilization of iron ore tailings as raw material for portland cement clinker production, Adv. Mater. Sci. Eng. 2016 (2016) 1–6, https://doi.org/10.1155/2016/1596047.

[18] G. Young, M. Yang, Preparation and characterization of Portland cement clinker from iron ore tailings, Constr. Build. Mater. 197 (2019) 152–156, https://doi.org/10.1016/j.conbuildmat.2018.11.236.

[19] V. Isteri, K. Ohenoja, T. Hanein, H. Kinoshita, H. Kletti, C. Rößler, P. Tanskanen, M. Illikainen, T. Fabritius, Ferritic calcium sulfoaluminate belite cement from metallurgical industry residues and phosphogypsum: clinker production, scale-up, and microstructural characterisation, Cem. Concr. Res. 154 (2022), 106715, https://doi.org/10.1016/j.cemconres.2022.106715.

[20] T.K. Chatterjee, Burnability and Clinkerization of Cement Raw Mixes, in: Adv. Cem. Technol., Elsevier, 1983: pp. 69–113. https://doi.org/10.1016/B978-0-08-028670-9.50009-0.

[21] R.H. Bogue, Calculation of the compounds in Portland cement, Ind. Eng. Chem. Anal. Ed. 1 (1929) 192–197, https://doi.org/10.1021/ac50068a006.

[22] H.F.W. Taylor, Cement chemistry, 2nd ed, T. Telford, London, 1997.

[23] A.K. Chatterjee, Chemico-Mineralogical Characteristics of Raw Materials, in: Adv. Cem. Technol., Elsevier, 1983: pp. 39–68. https://doi.org/10.1016/B978-0-08-028670-9.50008-9.

[24] A.K. Chatterjee, Cement Production Technology: Principles and Practice, 1 st, CRC Press, 2018.

[25] K. Zhang, Y. Lu, M. Rao, W. Zhang, F. Wang, Understanding the role of brownmilerite on corrosion resistance, Construction and Building Materials 254 (2020), 119262, https://doi.org/10.1016/j.conbuildmat.2020.119262.

[26] B.Z. Dilnesa, E. Wieland, B. Lothenbach, R. Dähn, K.L. Scrivener, Fe-containing phases in hydrated cements, Cem. Concr. Res. 58 (2014) 45–55, https://doi.org/10.1016/j.cemconres.2013.12.012.

[27] ABNT, ABNT NBR 10004, Solid waste - Classification (PT - BR), 2004.

[28] K. Scrivener, R. Snellings, B. Lothenbach (Eds.), A practical guide to microstructural analysis of cementitious materials, 1st ed., CRC Press, 2018. https://doi.org/10.1201/b19074.

[29] J.E. Post, D.L. Bish, Rietveld refinement of crystal structures using powder x-ray diffraction data, in: D.L. Bish, J.E. Post (Eds.), Mod. Powder Diffr., De Gruyter, 1989: pp. 277–308. https://doi.org/10.1515/9781501509018-012.

[30] W.D. Kingery, H.K. Bowen, D.R. Uhlmann, Introduction to Ceramics, John Wiley & Sons, 1976.

[31] Y. Kihara, Mineralogical study of Portland cement clinker (Estudo mineralógico de clínquer de cimento Portland, PT, BR), Master's degree, São Paulo University University of São Paulo 1978. https://doi.org/10.11606/D.44.1978.tde-02092013-095244.

[32] V.V. Timashev, The kinetics of clinker formation. The structure composition of clinker and its phases, 7th Int. Congr. Chem. Cem. (1980) 1–17.

[33] F.M. Lea, The Chemistry of Cement and Concrete, 3rd ed.,, Chemical Publishing, 1971.

[34] ABNT, ABNT NBR 16697, Portland Cement - Requirements (PT - BR), 2018.

[35] S. Brunauer, P.H. Emmett, E. Teller, Adsorption of gases in multimolecular layers, J. Am. Chem. Soc. 60 (1938) 309–319, https://doi.org/10.1021/ja01269a023.

[36] E. Standards, BS EN 197-1:2011 Cement Composition, specifications and conformity criteria for common cements, 2011.

[37] J.S. Raucci, R.T. Cecel, R.C.O. Romano, R.G. Pileggi, V.M. John, Effect of mixing method on the mini-slump spread of Portland cement pastes, Rev. IBRACON Estrut. E Mater. 11 (2018) 410–431, https://doi.org/10.1590/s1983-41952018000200010.

[38] M.H. Maciel, G.S. Soares, R.C.de O. Romano, M.A. Cincotto, Monitoring of Portland cement chemical reaction and quantification of the hydrated products by XRD and TG in function of the stoppage hydration technique, J. Therm. Anal. Calorim. 136 (2019) 1269–1284, https://doi.org/10.1007/s10973-018-7734-5.

[39] P.C.R.A. Abrão, F.A. Cardoso, V.M. John, Efficiency of Portland-pozzolana cements: water demand, chemical reactivity and environmental impact, Constr. Build. Mater. 247 (2020), 118546, https://doi.org/10.1016/j.conbuildmat.2020.118546.

[40] K. De Weerdt, M.B. Haha, G. Le Saout, K.O. Kjellsen, H. Justnes, B. Lothenbach, Hydration mechanisms of ternary Portland cements containing limestone powder and fly ash, Cem. Concr. Res. 41 (2011) 279–291, https://doi.org/10.1016/j.cemconres.2010.11.014.

[41] D18 Committee, Test Method for Determination of the Point Load Strength Index of Rock and Application to Rock Strength Classifications, ASTM International, n.d. https://doi.org/10.1520/D5731-16.

[42] F.C. Oliveira, M.P. Kassab, N.V. Silva, S.C. Angulo, L.M. Tavares, D.A. Lange, Probabilistic functions of mechanical properties of plain cement pastes determined by a reduced-size test, Construction and Building Materials 286 (2021), 122907, https://doi.org/10.1016/j.conbuildmat.2021.122907.

[43] N.V. Silva, S.C. Angulo, A. da Silva Ramos, D.A. Barboza, L.M.T. Lange, Improved method to measure the strength and elastic modulus of single aggregate particles, Mater. Struct. 52 (2019) 77, https://doi.org/10.1617/s11527-019-1380-7.

[44] N.V. Silva, Mechanical Properties of Phases and their Effects on the Mechanical Behavior of Concrete (PT - BR), São Paulo University, 2022.

[45] T.C. Powers, Studies of the physical properties of hardened portland cement paste, ACI J. Proc. 43 (1946). https://doi.org/10.14359/15302.

[46] B. Lothenbach, D.A. Kulik, T. Matschei, M. Balonis, L. Baquerizo, B. Dilnesa, G. D. Miron, R.J. Myers, Cemdata18: A chemical thermodynamic database for hydrated Portland cements and alkali-activated materials, Cem. Concr. Res. 115 (2019) 472–506, https://doi.org/10.1016/j.cemconres.2018.04.018.

[47] J.I. Bhatty, F.M. Miller, R.P. Boahn, Innovations in Portland Cement Manufacturing, 2nd edition, Portland Cement Assn, Skokie, Illinois, 2011.

[48] K. Dvořák, D. Všianský, S. Ravaszová, A. Jančíků, Synthesis of M1 and M3 alite polymorphs and accuracy of their quantification, Cem. Concr. Res. 163 (2023), 107016, https://doi.org/10.1016/j.cemconres.2022.107016.

[49] L. León-Reina, A.G. De la Torre, J.M. Porras-Vázquez, M. Cruz, L.M. Ordonez, X. Alcobé, F. Gispert-Guirado, A. Larrañaga-Varga, M. Paul, T. Fuellmann, R. Schmidt, M.A.G. Aranda, Round robin on Rietveld quantitative phase analysis of Portland cements, J. Appl. Cryst. 42 (2009) 906–916, https://doi.org/10.1107/S0021889809028374.
[50] I. Odler, Special Inorganic Cements, 1 st, CRC Press, London, 2000.
[51] F. Zunino, K. Scrivener, Factors influencing the sulfate balance in pure phase C3S/C3A systems, Cem. Concr. Res. 133 (2020), 106085, https://doi.org/10.1016/j.cemconres.2020.106085.
[52] K.L. Scrivener, A. Nonat, Hydration of cementitious materials, present and future, Cem. Concr. Res. 41 (2011) 651–665, https://doi.org/10.1016/j.cemconres.2011.03.026.
[53] L. Wadsö, M. Arndt, An international round robin test on isothermal (conduction) calorimetry for measurement of three-day heat of hydration of cement, Cem. Concr. Res. 79 (2016) 316–322, https://doi.org/10.1016/j.cemconres.2015.10.004.
[54] K.L. Scrivener, P. Juilland, P.J.M. Monteiro, Advances in understanding hydration of Portland cement, Cem. Concr. Res. 78 (2015) 38–56, https://doi.org/10.1016/j.cemconres.2015.05.025.
[55] C.F. Dunant, J. Granja, A. Muller, M. Azenha, K.L. Scrivener, Microstructural simulation and measurement of elastic modulus evolution of hydrating cement pastes, Cem. Concr. Res. 130 (2020), 106007, https://doi.org/10.1016/j.cemconres.2020.106007.
[56] F.M. Lea, P.C. Hewlett, M. Liska, Lea's chemistry of cement and concrete, Fifth edition, Butterworth-Heinemann, Oxford [England] ; Cambridge, MA, 2019.
[57] M. Laanaiya, A. Bouibes, A. Zaoui, Understanding why Alite is responsible of the main mechanical characteristics in Portland cement, Cem. Concr. Res. 126 (2019), 105916, https://doi.org/10.1016/j.cemconres.2019.105916.
[58] B. Lothenbach, G. Le Saout, E. Gallucci, K. Scrivener, Influence of limestone on the hydration of Portland cements, Cem. Concr. Res. 38 (2008) 848–860, https://doi.org/10.1016/j.cemconres.2008.01.002.
[59] T. Matschei, B. Lothenbach, F.P. Glasser, The AFm phase in Portland cement, Cem. Concr. Res. 37 (2007) 118–130, https://doi.org/10.1016/j.cemconres.2006.10.010.
[60] B.Z. Dilnesa, B. Lothenbach, G. Le Saout, G. Renaudin, A. Mesbah, Y. Filinchuk, A. Wichser, E. Wieland, Iron in carbonate containing AFm phases, Cem. Concr. Res. 41 (2011) 311–323, https://doi.org/10.1016/j.cemconres.2010.11.017.